# Crystallographic and Molecular-Modeling Studies of Lipase B from *Candida antarctica* Reveal a Stereospecificity Pocket for Secondary Alcohols[†,‡]

Jonas Uppenberg,[§] Niklas Öhrner,[∥] Martin Norin,[∥] Karl Hult,[∥] Gerard J. Kleywegt,[§] Shamkant Patkar,[⊥] Viggo Waagen,[#] Thorleif Anthonsen,[#] and T. Alwyn Jones*[,§]

*Department of Molecular Biology, Biomedical Centre, Uppsala University, Box 590, S-751 24 Uppsala, Sweden, Department of Biochemistry and Biotechnology, Royal Institute of Technology, S-100 44 Stockholm, Sweden, Novo Nordisk A/S, Novo Allé, DK-2880 Bagsværd, Denmark, and Department of Chemistry, The University of Trondheim, N-7055 Dragvoll, Norway*

*Received July 18, 1995*[⊗]

ABSTRACT: Many lipases are potent catalysts of stereoselective reactions and are therefore of interest for use in chemical synthesis. The crystal structures of lipases show a large variation in the shapes of their active site environments that may explain the large variation in substrate specificity of these enzymes. We have determined the three-dimensional structure of *Candida antarctica* lipase B (CALB) cocrystallized with the detergent Tween 80. In another crystal form, the structure of the enzyme in complex with a covalently bound phosphonate inhibitor has been determined. In both structures, the active site is exposed to the external solvent. The potential lid-forming helix α5 in CALB is well-ordered in the Tween 80 structure and disordered in the inhibitor complex. The tetrahedral intermediates of two chiral substrates have been modeled on the basis of available structural and biochemical information. The results of this study provide a structural explanation for the high stereoselectivity of CALB toward many secondary alcohols.

By definition, lipases (EC 3.1.1.3) hydrolyze triacylglycerols at one or more of the three ester bonds of these substrates (IUBMB, 1992). However, lipases are capable of hydrolyzing other types of substrate as well. Therefore, the distinction between lipases and other members of the carboxylic ester hydrolase family (EC 3.1.1) is not always clear. The lipases have, instead, been characterized by their drastically increased activity when acting at the lipid-water interface of a micellar or emulsified substrate [reviewed in Desnuelle (1972)]. This change in enzymatic activity is called interfacial activation.

In the past few years, the mechanism of lipase action has been studied from a new point of view following the crystal structure determination of a number of lipases (Brady *et al.*, 1990; Winkler *et al.*, 1990; Schrag *et al.*, 1991; Grochulski *et al.*, 1993; Noble *et al.*, 1993; Derewenda *et al.*, 1994a; Uppenberg *et al.*, 1994b). The structures of the lipase from *Rhizomucor miehei* and human pancreatic lipase were first determined without any substrates bound (Brady *et al.*, 1990; Winkler *et al.*, 1990). In both structures, a catalytic triad was identified, similar to the much studied triad found in serine proteases (Blow *et al.*, 1969; Wright *et al.*, 1969). In both lipases, the active site serine was buried under a helical lid and therefore was not accessible to external solvent. The structures of these enzymes with bound ligands revealed large conformational changes that opened the active site to the external solvent and created a hydrophobic surface appropriate for substrate binding (Brzozowski *et al.*, 1991; van Tilbeurgh *et al.*, 1993). A similar conformational change has been observed for *Candida rugosa* lipase where a *cis*−*trans* isomerization of a proline residue occurs in the lid region when the lid opens (Grochulski *et al.*, 1994).

Crystal structures of other enzymes from the esterase family, such as cutinase (Martinez *et al.*, 1992) and acetylcholinesterase (Sussman *et al.*, 1991), have also been solved. None of these enzymes have lids covering their active sites, however, nor do they display interfacial activation. The importance of a lid was also emphasized by a comparison of pancreatic lipase from human and guinea pig. The alignment of the amino acid sequence of guinea pig pancreatic lipase with that of the human enzyme suggested that the lid region was absent in the guinea pig sequence (Hjorth *et al.*, 1993). In contrast to other pancreatic lipases, the guinea pig enzyme does not display interfacial activation.

Most carboxylic ester hydrolases of known structure contain a Ser-His-Asp/Glu catalytic triad in the active site and share, at least in part, the common structural framework of the α/β-hydrolase fold (Ollis *et al.*, 1992). This fold is made up of a mostly parallel β-sheet, flanked on both sides by α-helices. The nucleophile is always found at the C-terminal edge of the sheet in a tight bend between a strand and a helix and can usually be identified from the consensus sequence G-x-(nucleophile)-x-G. The exceptions to this consensus include acetylcholinesterase (Sussman *et al.*, 1991), haloalkane dehalogenase (Franken *et al.*, 1991), *Candida antarctica* lipase B (CALB)[1] (Uppenberg *et al.*, 1994b), and thioesterase (Lawson *et al.*, 1994). A notable exception to the α/β-hydrolase fold is a *Streptomyces scabies*

[†] This investigation was carried out with financial support from Nordisk Industrifond, the Swedish Natural Science Research Council, and the Swedish Technical Research Council.

[‡] The atomic coordinates and structure factors have been deposited in the Protein Data Bank. The corresponding PDB codes are 1LBT (Tween 80 complex) and 1LBS (phosphonate inhibitor complex).

[§] Uppsala University.
[∥] Royal Institute of Technology.
[⊥] Novo Nordisk A/S.
[#] The University of Trondheim.

[⊗] Abstract published in *Advance ACS Abstracts,* December 1, 1995.

[1] Abbreviations: ncs, noncrystallographic symmetry; CALB, *Candida antarctica* lipase B; rms, root mean square.

0006-2960/95/0434-16838$09.00/0 

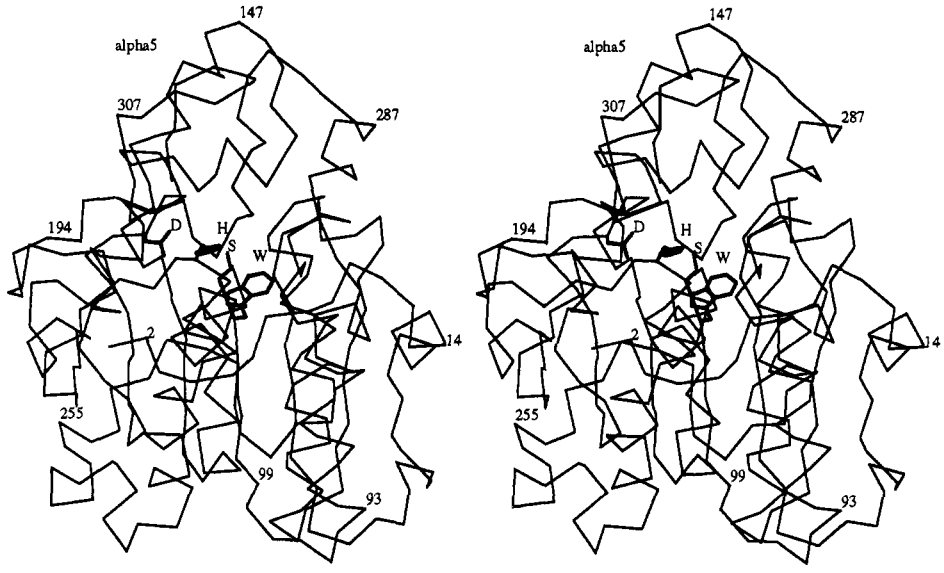


FIGURE 1: Stereotrace of the Cα atoms in CALB. The structure consists of a seven-stranded, mostly parallel β-sheet, surrounded by helices on both sides. The side chains of the catalytic residues Ser105, His224, and Asp187 are shown as well as the side chain of Trp104.

esterase, where the topology of the β-sheet is different and the acid in the catalytic triad is replaced by a carbonyl oxygen (Wei *et al.*, 1995).

Lipases have attracted much interest in recent years because of their potential use in industrial applications, for instance as additives to washing powder, in the production of rare oils and fats through transesterification, and for use in other types of organic synthesis (Gillis, 1988; Björkling *et al.*, 1991). They have also proven to be efficient stereoselective catalysts in the kinetic resolution of a wide variety of chiral compounds (Santaniello *et al.*, 1992). One of the most studied features of lipases is their ability to react selectively with one of two enantiomers of secondary alcohols. Empirical studies on different lipases and substrates have allowed the construction of a schematic model of the binding sites for the two substituents of the secondary alcohol (Kazlauskas *et al.*, 1991). By comparing the relative size of the two substituents of the alcohol, one could use this model to predict with high accuracy which of the two enantiomers would be converted faster by the lipase. The crystallographic work on lipases has permitted a more detailed investigation of their enantioselectivity. This was first done with the crystal structures of covalent complexes between *C. rugosa* lipase and (*R*)- and (*S*)-menthyl ester transition state analogues (Cygler *et al.*, 1994). These structures showed that the fast-reacting enantiomer could bind to the enzyme with an intact hydrogen bond between the alcohol oxygen and the Nε of the active site histidine. This bond was not formed with the slow-reacting enantiomer. The difficulty of the slow-reacting enantiomer in forming this hydrogen bond has been proposed to account for the enantioselectivity of this lipase as well as for that of other lipases and esterases (Cygler *et al.*, 1994). The latter conclusion was based on the observation that lipases share similar catalytic triads and alcohol binding sites.

CALB is a lipase with a 33 kDa molecular mass. It has proven to be a highly stereoselective enzyme for the kinetic resolution of secondary alcohols (Frykman *et al.*, 1993; Waagen *et al.*, 1993). We have previously reported the sequence and crystal structure of CALB in two crystal forms (Uppenberg *et al.*, 1994b). These structures revealed that the enzyme has an α/β-hydrolase-like fold, with an active site serine triad that is accessible from the solvent through a narrow channel (Figure 1). The open conformation of the enzyme in the absence of any substrate raised the question of whether CALB undergoes a conformational change upon activation. A short helix, α5, was identified as a potential lid on the basis of its position and an observed order/disorder in different crystal environments. A detergent molecule at the entrance of the active site channel could be removed by changing the pH of the crystals, and as a result, α5 changed from an ordered helix to disordered structure, manifested by a lack of continuous electron density. A similar disorder has been observed for the lid in the crystal structure of *Humicola lanuginosa* lipase (Derewenda *et al.*, 1994b).

We now present two new complex structures of CALB. In the first structure, CALB was incubated with the detergent Tween 80 prior to crystallization. In the second structure, the enzyme was inhibited by a racemic mixture of *n*-hexylchlorophosphonate ethyl ester (Björkling *et al.*, 1992). With information from these crystal structures and those of other lipase inhibitor complexes and assuming a reaction mechanism consistent with that of other serine hydrolases, we have modeled the tetrahedral intermediates of two acyl transfer reactions into the active site in order to explain the high stereoselectivity of CALB toward certain secondary alcohols. In the first intermediate, the underlying reaction is an interesterification with 1-phenylethanol as acyl acceptor and an octanoate ester as acyl donor (Frykman *et al.*, 1993). In the second intermediate, the modeled reaction is the hydrolysis of a glycerol butanoate derivative (Waagen *et al.*, 1993).

## MATERIALS AND METHODS

For the crystallographic work presented here, enzyme from the native organism was used exclusively. The purification of the native enzyme has been described elsewhere (Patkar *et al.*, 1993). CALB crystallizes under a variety of conditions (Uppenberg *et al.*, 1994a), but only the crystal forms relevant to this study will be presented here. All crystallization experiments were performed with the hanging drop method (McPherson, 1982), using silane-treated cover slips. The

Table 1: Data Collection and Processing Statistics

| | phosphonate[a] | Tween 80 |
|---|---|---|
| space group | $C2$ | $P2_1$ |
| cell axes (Å) | $a = 229.5, b = 95.6, c = 86.7$ | $a = 95.1, b = 50.2, c = 99.5$ |
| cell $\beta$-angle (deg) | 90.0 | 90.6 |
| molecules in asymmetric unit | 6 | 2 |
| $V_m$ (Å$^3$/Da) | 2.4 | 3.6 |
| resolution (Å) | 2.6 | 2.5 |
| highest shell (Å) | 2.69−2.60 | 2.59−2.50 |
| number of observations | 55 714 | 45 529 |
| unique reflections | 26 271 | 26 677 |
| completeness[b] (%) | 83 (55) | 82 (63) |
| $R_{merge}$[b,c] (%) | 5.0 (19.1) | 4.1 (12.3) |
| $\langle I/\sigma(I)\rangle$[b] | 13.0 (5.9) | 14.3 (6.0) |

[a] Reflections which were systematically absent due to the special noncrystallographic symmetry were removed before scaling the data and have been excluded from the statistics. [b] Values within parentheses were calculated for reflections in the highest resolution shell. [c] $R_{merge} = \sum_i\sum_j(|I_{ij} - \langle I_i\rangle|)/\sum i\sum_j|I_{ij}|$, where $I$ is the intensity, $i$ is an index for all unique reflections, and $j$ is an index for all observations of a unique reflection.

diffraction data for both complexes were collected at 20 °C on an SDMS Mark III multiwire area detector (Hamlin, 1985) mounted on a Rigaku rotating anode operating at 50 kV and 90 mA. The SDMS software was used for collection of the data, and the stored images were processed with MADNES (Messerschmidt & Pflugrath, 1987) and profile fitted with PROCOR (Kabsch, 1988). Scaling and merging of data were carried out with the Collaborative Computational Project Number 4 (CCP4) program package (CCP4, 1994). Statistics for the data sets are summarized in Table 1.

*Structure Determination of the CALB/Tween 80 Complex.* Prior to crystallization, the protein was incubated for 1 h at 37 °C with Tween 80, poly(oxyethylene) sorbitan monooleate. The Tween 80 concentration in the protein solution was 1−2 mM. Ammonium sulfate (1.0 M) was used as a precipitant together with 10% dioxane and 0.1 M sodium citrate/citric acid buffer (pH 4.0). The drop contained 5 $\mu$L of protein solution (10 mg/mL), 1 $\mu$L of $\beta$-octyl glucoside (4% w/v), and 1−2 $\mu$L from the reservoir. Crystals grew within a few days at 20−25 °C (Uppenberg *et al.*, 1994a). The space group is $P2_1$, and the cell constants are $a = 95.1$ Å, $b = 50.2$ Å, $c = 99.5$ Å, and $\beta = 90.6°$. There are two molecules in the asymmetric unit, and $V_m$ is 3.6 Å$^3$/Da (Matthews, 1968).

The structure was solved by molecular replacement with X-PLOR (Brünger, 1990) using a partially refined model from the monoclinic crystal form described earlier (Uppenberg *et al.*, 1994b) as a search model. The rotation function yielded two strong peaks, 7$\sigma$ and 5$\sigma$ above the mean. The translation functions also gave outstanding peaks, 8$\sigma$ and 9$\sigma$ above the mean, one for each rotation function solution. The correct origin relating the two molecules was found by evaluation of one-dimensional searches along the $b$ axis at each of the four possible origin choices for this space group. The structure was refined with X-PLOR (Brünger, 1992a) using force-field parameters derived from the Cambridge Structural Data Base (Engh & Huber, 1991). The initial model was based on the orthorhombic crystal form previously refined to 1.55 Å (Uppenberg *et al.*, 1994b). The progress of refinement was monitored with the free $R$-factor (Brünger, 1992b), with 5% of the data assigned to the test set. After rigid-body refinement, the $R$-factor was 29.3% and the free $R$-factor was 30.1% for reflections in the 8.0−3.0 Å range. Positional refinement by energy minimization as well as $B$-factor refinement were carried out with strict ncs constraints between the two molecules in the asymmetric unit, including ligand and waters. The ncs operator was obtained from the model after rigid body refinement. Water molecules, a partial Tween 80 molecule, and two $N$-acetylglucosamine residues at Asn74 were included per enzyme molecule. A few side chains were manually rebuilt with O (Jones *et al.*, 1991) to fit the averaged density (Kleywegt & Jones, 1994b). $B$-factor refinement was carried out with main chain atoms and side chain atoms grouped for each residue. Well-connected density for part of the Tween 80 ligand was observed in the active site. In an attempt to improve the density, high-temperature simulated annealing calculations (Brünger *et al.*, 1987) in which harmonic positional restraints were used for all non-hydrogen atoms were carried out. The rationale behind this approach was to tether the protein structure to its starting conformation (*i.e.* the high-resolution structure), except for areas where the crystallographic data of the complex provided a sufficiently large driving force to effect changes. The model phases improved sufficiently to reveal well-connected density for a Tween 80 molecule extending all the way out to the solvent interface. A partial model of a Tween 80 molecule was built and fitted to the density. The resulting model was subjected to another high-temperature simulated annealing calculation, again using harmonic positional restraints for all atoms except those of the ligand. The final model has an R-factor of 17.1% for reflections between 7.5 and 2.5 Å, and the free $R$-factor is 19.4%. The rms deviation from the orthorhombic model is 0.22 Å for Cα's and 0.25 Å for all non-hydrogen atoms. Refinement and model quality statistics are summarized in Table 2. A plot of the real-space fit of the model to the final $2F_{obs} - F_{calc}$ map and of the main chain $B$-factors is shown in Figure 2. The active site Ser 105 adopts an energetically strained conformation typical for $\alpha/\beta$-hydrolases, with main chain dihedral angles $\phi = 52.0°$ and $\psi = -119.0°$.

*Structure Solution of the CALB/Phosphonate Inhibitor Complex.* CALB was inhibited effectively by a racemic mixture of the phosphonate inhibitor in equimolar amounts (Patkar *et al.*, 1993). The protein complex was crystallized at room temperature. The reservoir contained 1.3 M ammonium sulfate as precipitant, 0.1 M sodium citrate/citric acid buffer (pH 4.0) and 10% dioxane. The drop contained 5 $\mu$L of protein solution (10 mg/ml), 1 $\mu$L of 4% $\beta$-octyl glucoside, and 1 $\mu$L from the reservoir. The space group is $C2$, and the cell constants are $a = 229.5$ Å, $b = 95.6$ Å, $c = 86.7$ Å, and $\beta = 90.0°$. There are six molecules in the asymmetric unit, and $V_m$ is 2.4 Å$^3$/Da.

This crystal form exhibits unusual local symmetry, which manifests itself by systematic absences in the diffraction pattern and by high peaks in the self Patterson map. There is one peak at ($^1/_3$,0,$^1/_3$) and another at ($^1/_3$,0,$-^1/_3$), which are of unequal height. The relative heights of these peaks also vary between data sets collected from different crystals, and these data sets do not merge well. While individual data sets can be merged with internal $R$-factors of less than 5%, combining data sets from different crystals gives merging $R$-factors of more than 25%. This suggested that the crystals suffered from merohedral twinning; in which case, two

Table 2: Refinement and Model Statistics

| | phosphonate | Tween 80 |
|---|---|---|
| resolution limits (Å) | 7.5−2.6 | 7.5−2.5 |
| highest shell (Å) | 2.69−2.60 | 2.59−2.50 |
| number of reflections ($F > 0$) | 15 621 | 25 979 |
| completeness (%) | 82[a] | 82 |
| *B*-factor model | grouped | grouped |
| NCS model | 6-fold constrained | 2-fold constrained |
| *R*-factor[b] (%) | 20.7 (29.9) | 18.7 (25.2) |
| *R*-free[c] (%) | 26.5 (35.1) | 20.9 (30.9) |
| number of atoms ($Z > 1$) | | |
| protein | 2324 | 2324 |
| active site ligand | 11 | 36 |
| carbohydrates | 28 | 28 |
| water molecules | 92 | 155 |
| rms deviations from ideal geometry[d] | | |
| bond lengths (Å) | 0.020 | 0.007 |
| bond angles (deg) | 2.2 | 1.3 |
| dihedral angles (deg) | 25.0 | 23.7 |
| improper torsion angles (deg) | 2.0 | 1.3 |
| average *B*-factors (Å$^2$) | | |
| main chain atoms | 17.5 | 13.7 |
| all protein atoms | 18.1 | 15.4 |
| active site ligand | 20.5 | 54.8 |
| carbohydrates | 46.3 | 68.8 |
| water molecules | 27.6 | 40.2 |

[a] In the calculation of the completeness for the phosphonate data set, the total number of possible reflections was calculated as the number of reflections for the major twin component that were not systematically absent due to the special local symmetry. [b] *R*-factor = $\sum_h||F_{obs}| - |F_{calc}||/\sum_h|F_{obs}|$, where $F_{obs}$ and $F_{calc}$ are the observed and calculated structure factors, respectively. [c] *R*-free has the same definition as *R*-factor, but calculated for a subset of reflections not used in the structure refinement. [d] Values calculated with X-PLOR. Parameters derived from the Cambridge Database of small molecule structures (Engh & Huber, 1991) were used for the bond lengths and bond angles.

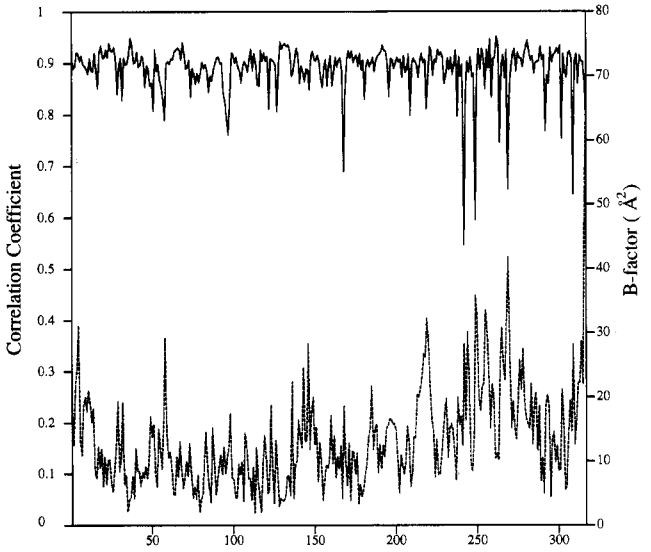


FIGURE 2: Real-space fit diagram (Jones *et al.*, 1991) of the final model of the Tween 80 complex (solid line). The correlation coefficient was calculated using an unaveraged $2F_{obs} - F_{calc}$ map. The lower curve shows the main chain *B*-factors of the residues.

independent crystal lattices overlap, and the observed intensities are the sums of intensities from the two lattices (Fisher & Sweet, 1980). In this case, the two twins are related by a 180° rotation around the *x* or *z* axis. The absences due to noncrystallographic symmetry can be explained by positioning three molecules with the same orientation in the unit cell at coordinates $(x,y,z)$ for molecule 1, $(x+^1/_3,y,z+^1/_3)$ for molecule 2, and $(x+^2/_3,y,z+^2/_3)$ for molecule 3. The two twin components generate different sets of absent reflections with the result that some reflections can be attributed to one lattice only, whereas other reflections have intensity contributions from both lattices (Figure 3). Prior to refinement of the structure, the data set was modified so that only the contribution from the larger twin component remained. Those reflections for which both twins contributed to the intensities were modified according to the method described by Fisher and Sweet (1980). This requires knowledge of the relative sizes of the twin components. These were calculated from the relative heights of the translation peaks in the self Patterson function. In the crystal used, the relative sizes were 0.296 and 0.704 for the small and large twin component respectively. Since the unit cell $\beta$-angle is exactly 90°, there are two possible ways to index the data. We have arbitrarily chosen the indexing that results in a $(^1/_3,0,^1/_3)$ translation in the asymmetric unit for the modeled twin component.

The structure was solved by molecular replacement methods using X-PLOR. The rotation function resulted in two outstanding peaks, both $13\sigma$ above the mean, which were related by a 2-fold rotation around an axis parallel to the crystallographic *a* axis. The translation functions for the two orientations gave many peaks, the highest in each being $12\sigma$ above the mean, which were related by the translations described above. Combining this information with the crystallographic symmetry, we constructed an asymmetric unit with six enzyme molecules (Figure 4). The positions and orientations of the individual molecules were improved with rigid-body refinement, followed by positional refinement and grouped *B*-factor refinement using strict ncs constraints. Ninety-two solvent molecules per enzyme molecule were identified in an averaged $2F_{obs} - F_{calc}$ map. The N-glycosylation site on Asn74 showed density for two carbohydrate molecules. A few side chains showed different conformations compared to the initial model and were rebuilt with O. In the last step of the refinement, the inhibitor was added to the model according to the density. The final *R*-factor is 20.9% for reflections between 7.5 and 2.6 Å resolution, and the free *R*-factor is 26.5% using 10% of the reflections as the test set. Density can be seen for most of the structure, except around helix α5 where a number of side chains have poor or no density. This is reflected in the graph of the real-space fit and *B*-factors (Figure 5). The final model has an rms deviation of 0.33 Å from the initial orthorhombic model for Cα's and 0.42 Å for all nonhydrogen atoms. Refinement and model quality statistics are summarized in Table 2. The rms deviations from ideal bond lengths and angles are higher than we usually obtain with this refinement protocol and may be due to the special nature of this crystal form. The main chain dihedral angles for Ser105 are $\phi = 54.5°$ and $\psi = -110.0°$. A test calculation in which residues 128−132 (corresponding to a normally well-determined part of the structure) were omitted from the model prior to rigid-body refinement and energy minimization was also carried out. The resulting model was used to calculate an $F_{obs} - F_{calc}$ map which was averaged over the six molecules in the asymmetric unit. The omitted region of the model clearly matches the density as shown in Figure 6.

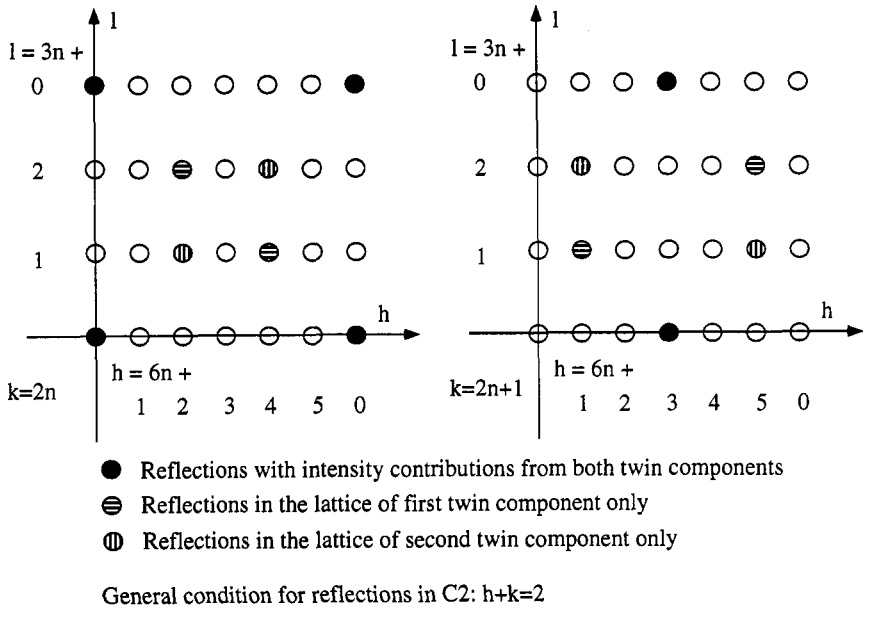


FIGURE 3: Reflections in the phosphonate inhibitor data set can be partitioned into different subsets, because of the special noncrystallographic symmetry and the merohedral twinning. The molecules in the asymmetric unit are related by pure translations in the *a/c* plane, which results in a number of systematic absences in the diffraction pattern. The sets of absences are partly different for the two twin components in the crystal, which makes it easy to separate them for parts of the data. Some reflections have to be corrected to remove the contribution from the unwanted twin.

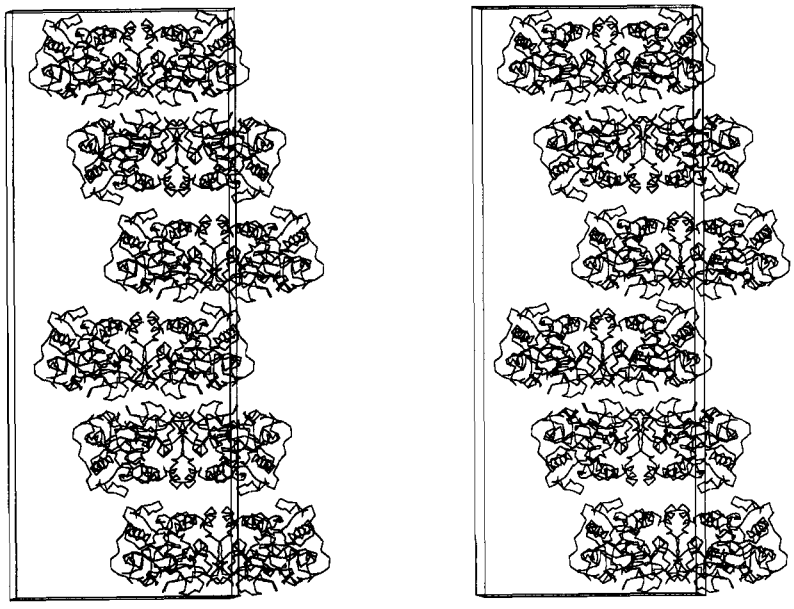

FIGURE 4: CALB/phosphonate inhibitor complex packs with six molecules in the asymmetric unit. They are arranged as three closely packed dimers, in which the hydrophobic surfaces of the molecules face each other. The structural dimer is practically identical to that found in the monoclinic crystal form described earlier (Uppenberg *et al.*, 1994b). The stereofigure shows two asymmetric units related by the crystallographic centering operation.

*Molecular Modeling and Dynamics Simulations.* Models of the substrates were constructed and energy minimized with the Biosym Insight II software on a Silicon Graphics workstation. The initial manual modeling was performed in O on an Evans and Sutherland ESV workstation. Molecular dynamics simulations, energy minimizations, manipulations of molecules, and graphic evaluations were done with the Tripos SYBYL version 6.03 molecular-modeling program on an Evans and Sutherland ESV workstation.

The environment of the lipase was modeled as vacuum to make the computations feasible (Norin *et al.*, 1994a). The AMBER force field (Weiner *et al.*, 1984,1986), using a distance dependent dielectric constant and a nonbonded cutoff distance of 10 Å, was used in all energy minimizations and molecular dynamics simulations. Energy minimizations were performed with the Powell minimizer in SYBYL. The molecular dynamics simulations were performed using a time step of 2 fs, with constraints on all bond lengths using the SHAKE algorithm (Ryckaert *et al.*, 1977).

The GRID program (Goodford, 1985) calculates the energy potentials for various functional groups around a protein. This program was used to map possible substrate interactions in the active site and to assign strongly bonded water molecules which are not replaced by solvent molecules when reactions are performed in an organic solvent. A GRID calculation with a water probe was used to obtain a contour plot at −6.5

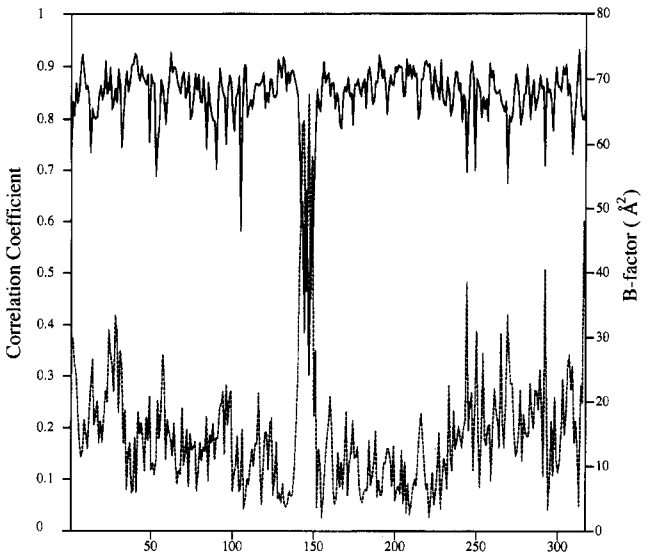


FIGURE 5: Real-space fit diagram (Jones *et al.*, 1991) for the final model of the phosphonate inhibitor complex. An unaveraged $2F_{obs} - F_{calc}$ map was used for the calculation. The lower curve shows the main chain *B*-factors of the residues. The disorder of helix α5 is manifested by poor real-space fit values and high *B*-factors.

kcal/mol on the graphics display, together with the crystal structure. All water molecules in the X-ray crystal structure which were located inside the energy contour, 160 out of 283, were included in the molecular dynamics simulations. Polar hydrogens were added using the BIOPOLYMER module of the SYBYL program, and the structure was energy minimized. In the first minimization (150 steps), only the water molecules were allowed to move. In the next minimization (2200 steps), all atoms were allowed to move. The minimized structure was used in molecular dynamics simulations in which all atoms within 6 Å of the Oγ atom in the active site serine were allowed to move and were represented by the all-atom AMBER force field (Weiner *et al.*, 1986). Additional hydrogens were added by the BIOPOLYMER module of the SYBYL program. Outside the 6 Å sphere, the united atom AMBER force field (Weiner *et al.*, 1984) was applied. Between 6 and 10 Å, all atoms were allowed to move. Between 10 and 14 Å, only the side chains of the amino acid residues and the water molecules were allowed to move. Outside the 14 Å sphere, all atoms were constrained to their positions in the starting structure. Partial charges for the atoms of the transition state residues were calculated by a semiempirical method (Besler *et al.*, 1990) using the MOPAC 6.0 ESP program.

Starting models of enzyme−substrate transition states were built as tetrahedral covalent complexes with the Oγ atom of the active site serine residue connected to the carbonyl carbon atom of the substrate (Figure 7). In agreement with the bi−bi ping−pong reaction mechanism, a protonated histidine residue in the catalytic triad was assumed to be present in the transition state (Martinelle & Hult, 1995). In this reaction mechanism, the protonated active site histidine forms hydrogen bonds to the Oγ of the catalytic serine and to the oxygen of the alcohol group of the substrate. Furthermore, the oxyanion of the transition state intermediate should interact with the oxyanion hole of the active site. These rules constrained the docking procedure. Energy contour maps from the GRID calculations using a methyl probe helped in adjusting the torsion angles of the remaining part of the substrate.

The energies and structures of the substrate/enzyme complexes were calculated by a combined energy minimization and molecular dynamics protocol, previously employed in calculations of substrate/chymotrypsin complexes (Norin *et al.*, 1993) and substrate/lipase complexes (Norin *et al.*, 1994b). Energy minima of the substrate/lipase complexes were found by molecular dynamics simulations in vacuum, in which the molecules were repeatedly heated to 300 K and slowly cooled to 1 K. The starting models of the transition state intermediates were subjected to 500 steps of energy minimization before the molecular dynamics simulations. After an initial equilibration in which the structures were heated during 1.2 ps to 300 K and thereafter equilibrated during 10 ps at 300 K, the temperature of the system was

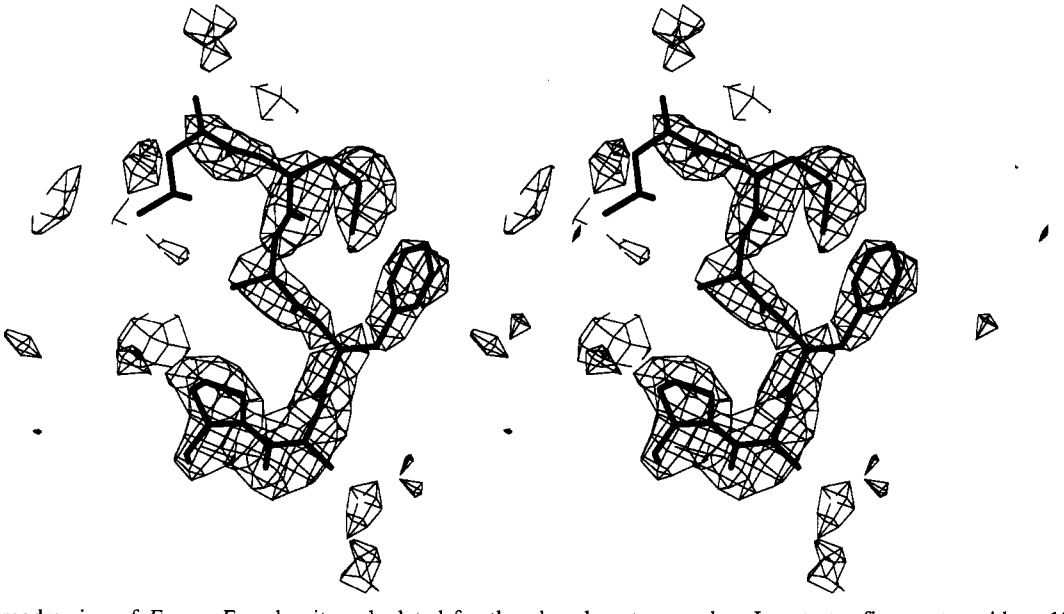

FIGURE 6: Stereodrawing of $F_{obs} - F_{calc}$ density calculated for the phosphonate complex. In a test refinement, residues 128−132 were omitted from the model prior to rigid-body refinement and energy minimization. The map shows density for the omitted part of the structure, and for Pro133, a residue that moved away from its original position in this refinement.

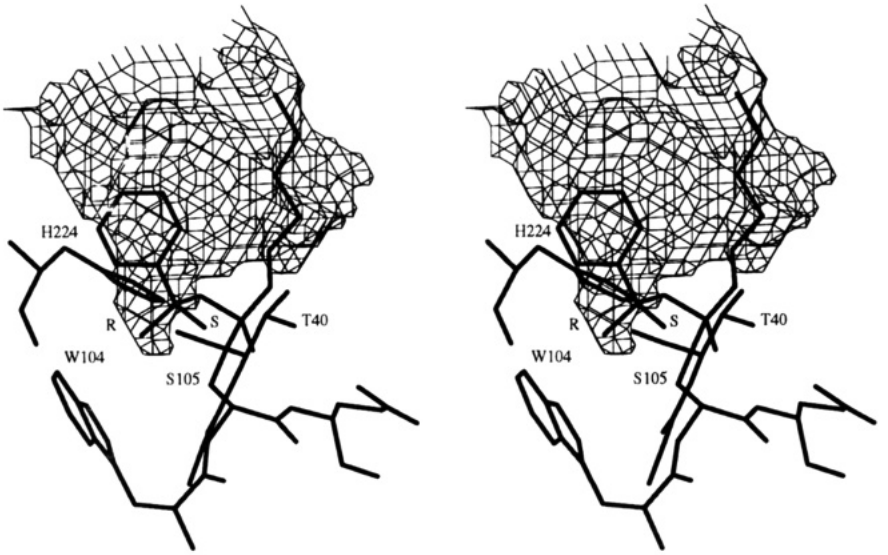


FIGURE 7: Stereodrawing of the solvent accessible surface of the active site pocket and a 1-phenylethyl octanoate modeled as a tetrahedral intermediate. Both the *R* and *S* enantiomers are shown, labeled at the methyl group at which they differ. In the *R* enantiomer, the methyl group is pointing into the stereospecificity pocket. In the *S* enantiomer, it points towards the backbone atoms of Gly39 and Thr40, making many close contacts. The hydrogen bond between the histidine and the alcohol oxygen is also indicated. The surface was calculated with a 1.4 Å probe radius using VOIDOO (Kleywegt & Jones, 1994a).

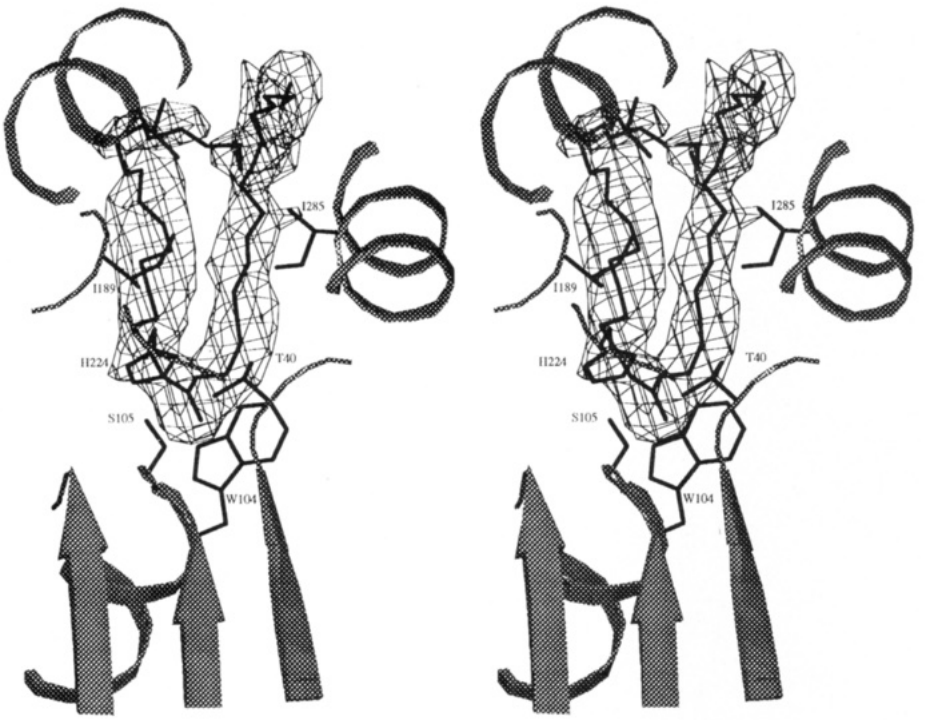


FIGURE 8: Stereodrawing of $F_{obs} - F_{calc}$ density in the active site pocket of the Tween 80 complex. The Tween 80 molecule was not included in the map calculation. The partial Tween 80 molecule from the final model is also shown.

decreased during 1.5 ps to 1 K. Then the temperature was raised during 1.2 ps to 300 K, followed by equilibration during 6 ps before the next cooling period. Ten cycles of heating and cooling were run. The total simulation time was 98 ps. The conformations trapped at 1 K were subjected to 500 steps of energy minimization.

## RESULTS

### *Crystallography*

*Crystal Structure of CALB Cocrystallized with Tween 80.* This structure shows two approximately parallel tubes of density, originating at the active site serine and leading out to the surface of the molecule (Figure 8). The Tween 80 molecule (Figure 9) is a monoester that can account for the observed density, although the complete substrate molecule cannot be modeled. We have modeled the Tween 80 molecule in the active site pocket as an ester prior to hydrolysis. In order to be hydrolyzed, the alcohol oxygen of the substrate must be able to receive a proton from N$\epsilon$ of the active site histidine. We have used this biochemical restriction to assign the two chains of the substrate to the two tubes of density. The putative lid $\alpha$5 adopts the same conformation as observed in the previously reported CALB crystal forms and shows no sign of disorder (Figure 2). The packing in these crystals is different from that of all other

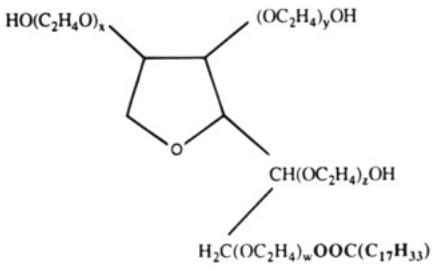


FIGURE 9: Tween 80 is a nonionic detergent with an approximate molecular mass of 1.3 kDa. The sum of $x$, $y$, $z$, and $w$ is ~20. The oleate part of the substrate is shown in bold.

crystal forms that have been determined, and the solvent content of ~63% is unusually high. It is also the only crystal form in which the hydrophobic surface around the active site pocket is almost fully accessible to the solvent. The high concentration of Tween 80 in the solution may have contributed to the exposure of this surface.

*Crystal Structure of CALB in Complex with the Phosphonate Inhibitor.* The dimeric packing motif, found in the earlier monoclinic crystal form (Uppenberg *et al.*, 1994b), reappears in this structure (Figure 4), although the unit cells and space groups are different. In this crystal form, α5 is again disordered, with 4−5 residues displaying weak electron density. There is additional electron density in the active site which we have assigned to the inhibitor. This density suggests a covalent attachment to the catalytic serine, Ser105, as predicted for this compound (Björkling *et al.*, 1992). There are two tubes of density of unequal length which extend from a large spherical feature in the density connected to the serine hydroxyl (Figure 10). Clear density is also present for an atom pointing toward the oxyanion hole. The phosphonate inhibitor has side chains extending from the phosphorus atom, with the acyl part being a hexyl group and the alcohol part an ethoxy group (Figure 11). This compound could be fitted completely into the density (Figure 10). However, the shorter tube contains some extra density, in which another atom can be positioned. At the resolution of this study, it cannot be ruled out that both enantiomers of the inhibitor bind competitively to the serine. This would give rise to a mixture of conformations for the acyl and alcohol parts of the inhibitor in the active site pocket. In the hydrolysis of an ester substrate, the alcohol oxygen receives a proton from the active site histidine and must therefore be within hydrogen bonding distance from the Nε of this residue. In the reaction of the inhibitor with the enzyme, the alcohol oxygen does not take part in the reaction. The enzyme's preference for one of the two enantiomers is therefore governed predominantly by the size of the two side chains and their ability to make favorable interactions in the active site pocket of the enzyme. The observed density suggests that the enzyme has been inhibited primarily with the enantiomer which does not form a hydrogen bond with the Nε of the active site histidine. The other enantiomer can also be modeled into the active site, albeit with density missing for parts of its acyl chain. This alternative interpretation of the electron density supplies information for the modeling of a tetrahedral intermediate for this enzyme.

### *Modelling of Chiral Substrates*

CALB has been used for kinetic resolution of chiral secondary alcohols, both in hydrolysis of esters and in ester synthesis. In many of these reactions, CALB displays a very high degree of stereoselectivity. To provide a structural

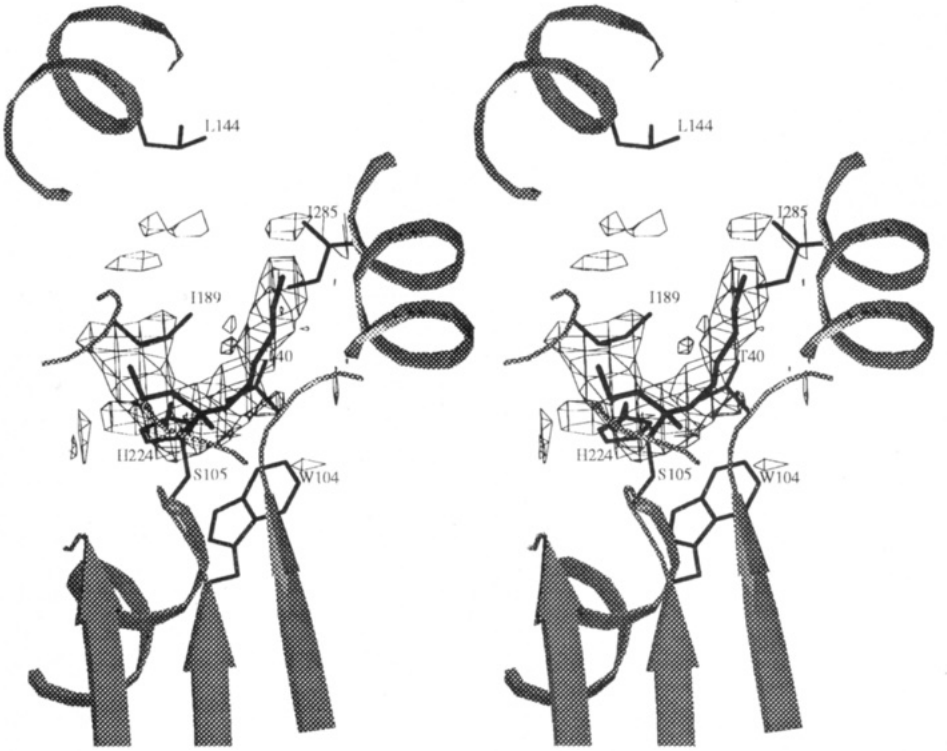


FIGURE 10: Stereodrawing of averaged $F_{obs} - F_{calc}$ density for the phosphonate inhibitor complex. The map was calculated with a model in which the inhibitor molecule had not yet been included. The inhibitor binds covalently to the active site serine. It is located in the active site pocket, with the alcohol oxygen in a position that would not be favorable for catalysis in an analogous substrate. If the acyl and alcohol parts of the inhibitor traded positions, the inhibitor would represent the alleged tetrahedral intermediate of an ester substrate better, with a hydrogen bond between the active site histidine and the alcohol oxygen. Density can also be seen for the inhibitor oxygen in the oxyanion hole. The map was averaged with programs in the RAVE package (Kleywegt & Jones, 1994b).

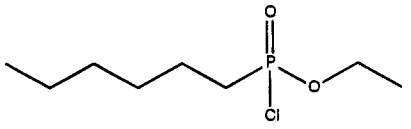

FIGURE 11: The phosphonate inhibitor used here is a racemic mixture of *n*-hexylchlorophosphonate ethyl ester. The chlorine atom is released when the inhibitor reacts with the enzyme.

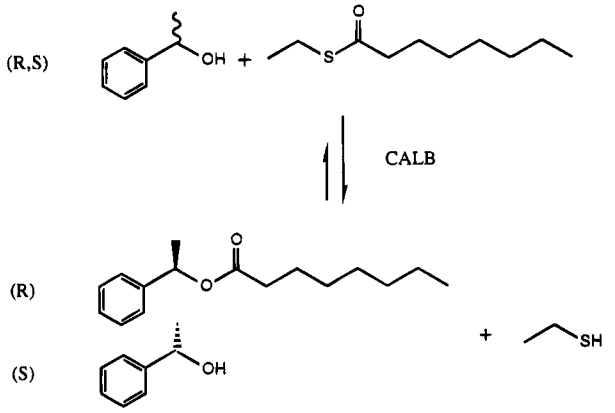


FIGURE 12: Substrate 1: phenylethyl octanoate. The stereoselective resolution of 1-phenylethanol is very high in CALB, as only the *R* enantiomer of the alcohol reacts with the enzyme. The reaction was carried out at 39 °C, under atmospheric pressure, in order to shift the reaction equilibrium in favor of the forward reaction. For a detailed description of the experimental conditions, see Frykman *et al.* (1993).

explanation for this phenomenon, we have carried out a series of molecular-modeling experiments.

*Substrate 1: 1-Phenylethyl Octanoate.* The first reaction step to be modeled was the formation of the tetrahedral intermediate of the esterification of racemic 1-phenylethanol into 1-phenylethyl octanoate. This reaction (Figure 12) strongly favors the *R*-enantiomer of the alcohol with an observed enantiomeric ratio, *E*, greater than 200 (Frykman *et al.*, 1993). First, we modeled the atoms associated with the tetrahedral carbon of the intermediate. For this, we used the crystal structure of *R. miehei* in complex with the inhibitor *n*-hexylphosphonate ethyl ester (Brzozowski *et al.*, 1991). This structure was aligned with CALB to give an optimal fit with respect to the active site residues and the residues forming the oxyanion hole. For modeling the alcohol, we took into account the geometric restrictions inherent in the tetrahedral intermediate. Thus, we assumed that the position of the carbonyl carbon and the oxyanion as well as the oxygen and the neighboring (chiral) carbon on the alcohol group must be relatively fixed in order to allow for the transfer of a proton between the active site histidine and the alcohol oxygen. The corresponding atoms from the *R. mucor* inhibitor were therefore assumed to represent a good starting model. The electron density from the CALB/inhibitor complex also supports such a positioning of these atoms.

These constraints leave only one degree of rotational freedom to fit the remaining part of the alcohol in the active site. This was done manually with guidance from the density seen in the active site channel in the Tween 80 crystal form and the van der Waals surface of the surrounding protein (Figure 7). This led to one unique orientation with the phenyl group pointing out toward the protein surface in both the *S* and the *R* form. What remained to be examined was the orientation of the methyl group of the chiral carbon for the two enantiomers. In the *R* enantiomer, this methyl group fits nicely into a small pocket that is delimited by the main chain of the third strand on one side and by the side chain of Trp104 on the other. In the *S* enantiomer, the methyl group is pointing toward the main chain atoms of Gly39 and Thr40 and the substrate oxyanion, and it makes many close van der Waals contacts. These steric clashes make this interaction highly unfavorable, especially since the two residues are involved in oxyanion stabilization (Figure 7). The acyl side of the enzyme/substrate complex was fit manually to the observed density of the CALB/inhibitor complex.

*Energy Minimization and Molecular Dynamics of Substrate 1.* To allow this model to relax, we carried out a number of molecular dynamics simulations. This was done to identify regions where close contacts could be relaxed by changes in conformation in either protein or intermediate and to help formulate test hypotheses. The minimized structures with the lowest energy are shown in Figure 13 for both enantiomers. The orientation of the alcohol moiety in the *S* enantiomer differed substantially from that in the starting structure. The methyl group moved into the small pocket, and the phenyl group pointed out toward the protein surface. These rearrangements moved the alcohol oxygen atom toward the oxyanion hole, thereby breaking the catalytically essential hydrogen bond to His224. This suggests that, in a transesterification reaction, the *S* alcohol cannot easily donate a proton to the catalytic histidine residue which is essential for nucleophilic attack on the acyl enzyme. Consequently, in a hydrolysis reaction, the alcohol moiety of the substrate would be stuck in a position where it cannot accept a proton from the catalytic histidine and is therefore not an efficient leaving group. In contrast, the energy minima of the tetrahedral intermediate of the *R* enantiomer contain a favorable hydrogen bond between the catalytic histidine and the oxygen atom of the alcohol group which would enable rapid proton transfer during catalysis.

*Substrate 2: Butanoate of a Glycerol Derivative.* In another study, CALB has been used for enantiomeric resolution of a glycerol monoester derivative by hydrolysis of the *sn*-2 ester bond (Waagen *et al.*, 1993). This substrate is similar to phenylethyl octanoate in the sense that it contains a chiral carbon on the alcohol group at the same position relative to the carbonyl carbon (Figure 14). The two free groups extending from this chiral carbon are a methoxymethyl group and a phenyl-containing group. In this hydrolytic reaction, the *R* enantiomer of the substrate is the favored enantiomer, with an enantiomeric ratio exceeding 100.

The *R* enantiomer was modeled with its methoxymethyl group pointing into the small stereospecificity pocket, although this gave rise to a few close contacts with the side chain of Trp104. The long side chain could be positioned in the channel leading out to the protein surface. The *S* enantiomer was more difficult to position, and the long side chain of the alcohol had to be curved in order to avoid close contacts with the protein.

*Energy Minimization and Molecular Dynamics of Substrate 2.* The enzyme/substrate complex was subjected to the same molecular dynamics simulation and energy minimization protocol as the first complex. In the resulting minimized structure, the bonds in the carbon chain of the large group of the fast-reacting *R* enantiomer were all in relaxed *trans* conformations. The small group was interact-

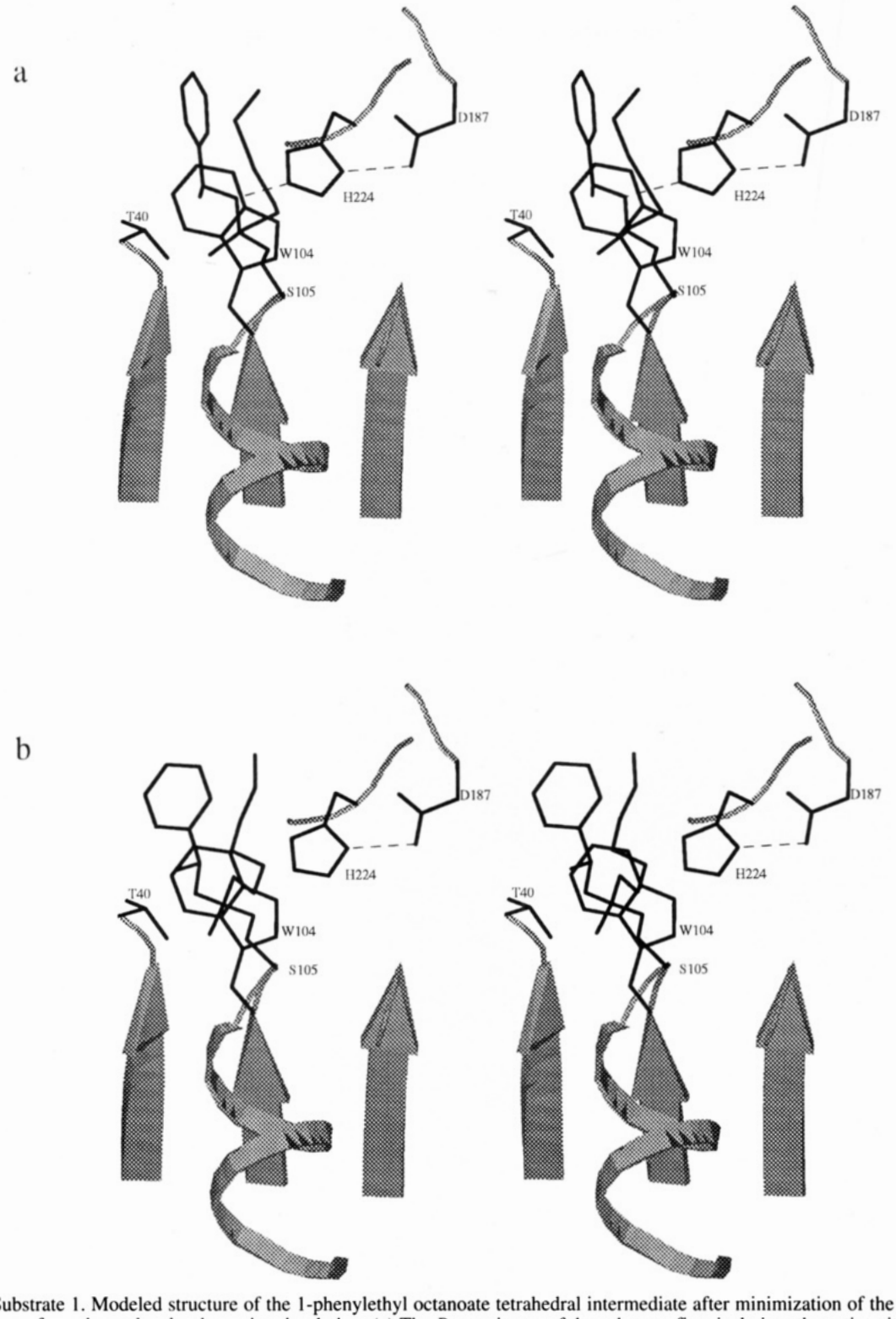


FIGURE 13: Substrate 1. Modeled structure of the 1-phenylethyl octanoate tetrahedral intermediate after minimization of the structure with the lowest energy from the molecular dynamics simulation. (a) The *R* enantiomer of the substrate fits nicely into the active site pocket, with the hydrogen bond between the histidine and the substrate intact. (b) The *S* enantiomer adopts a conformation in which the two free groups of the alcohol have a conformation similar to those in the *R* enantiomer. However, the alcohol oxygen points away from the active site histidine, making a proton transfer between these two groups impossible.

ing with Trp104 in the small pocket. This was possible by a small adjustment of the side chain of Trp104, which was pushed back slightly toward the interior of the protein (Figure 15a). The large group of the slow-reacting *S* enantiomer was twisted away from the specificity pocket, mainly interacting with the side chains of Leu278, Ala282, and Ile285 (Figure 15b). The presence of these side chains forced the carbon chain of this group of the substrate to adopt an energetically less favorable conformation. The small group occupied a space between the large alcohol side chain and the carbon chain of the acyl group, and the small pocket is empty. The acyl group moved toward the bottom of the active site. The slow-reacting *S* enantiomer retained the hydrogen bond between the histidine residue of the catalytic triad and the oxygen atom of the alcohol group. It is possible that the chiral preference for the *R* enantiomer is due partly

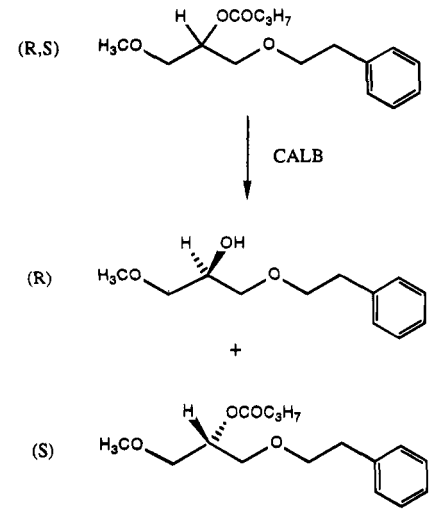


FIGURE 14: Substrate 2: butanoic ester of 1-(2-phenylethyl) ether of 3-methoxy-1,2-propanediol. This compound can be resolved efficiently by hydrolysis, using CALB as a catalyst. As for substrate 1, the enzyme reacts preferably with the *R* enantiomer, with the enantiomeric ratio for the reaction exceeding 100 (Waagen *et al.*, 1993).

to the relaxed conformation of the large group compared to the strained conformation of the *S* enantiomer, although it does not necessarily explain the high enantiomeric ratio for this substrate.

## DISCUSSION

The two new crystal structures of CALB indicate how a substrate can fit into the active site and be hydrolyzed by this enzyme. The environment of the active site appears unchanged compared to those of our previously determined structures. The structure of the Tween 80 complex suggests that the ideal substrate for hydrolysis is a monoester, which can be fitted with the acyl and alcohol moieties each occupying one of the two channels that can be distinguished in the active site pocket. Because of the restrictions inherent in the reaction mechanism, in which a proton must be transferred from the active site histidine to the alcohol oxygen of the substrate, the positioning of the two substrate side chains can be unambiguously assigned to the two active site channels. We have therefore termed these two channels the acyl side and the alcohol side of the active site pocket (Figure 16). These two channels run almost parallel from the active site serine to the surface and are just barely separated by two hydrophobic side chains, Ile189 and Ile285. It is difficult to envisage how a triglyceride with three long acyl chains could be fitted into the active site without a large conformational change taking place in the protein.

The phosphonate inhibitor structure confirms the role of Ser105 as the catalytic serine in this serine hydrolase. The density for the inhibitor suggests that it binds primarily to the active site serine, with the acyl part of the substrate in the alcohol side of the pocket and *vice versa*. This structure is therefore not a good model for a tetrahedral intermediate of the enzyme. The extra density on the acyl side of the pocket may indicate that both enantiomers of the inhibitor are bound to the enzyme. The CALB/inhibitor complex can be compared with the structure of *R. miehei* lipase in complex with the same inhibitor (Brzozowski *et al.*, 1991). In this structure, only one conformation of the inhibitor was observed in the active site, and it is believed to mimic the tetrahedral intermediate of the corresponding substrate.

In other lipase structures, different kinds of lids shield the active site from the outside solvent when no substrate is present. Such a closed form has not been observed for CALB, although we have earlier identified helix α5 as a candidate for such a function (Uppenberg *et al.*, 1994b). In the monoclinic crystal form described in our previous study, α5 becomes disordered when the pH is raised in the crystal and a β-octyl glucoside molecule is released from the active site. The disorder manifests itself by the disappearance of the electron density for this helix. In the orthorhombic form, the helix is well-ordered and a leucine side chain of a crystallographically related molecule points into the hydrophobic tunnel that leads to the active site. The structure of the CALB/phosphonate complex shows disorder for α5 that is reminiscent of the disorder in the monoclinic crystal form described above. In the CALB/Tween 80 structure, however, α5 is well-ordered. In this crystal form, both Tween 80 and β-octyl glucoside are present in the crystallization drop. In the previous monoclinic form, the density for the β-octyl glucoside is positioned on the acyl side of the active site pocket. The parallel tubes of electron density that we now observe leading from the active site have, therefore, been modeled as a partial Tween 80 molecule. Both Tween 80 and β-octyl glucoside have long, unbranched chains that would extend well outside the active site pocket. With this information, one could argue that helix α5 can be stabilized by hydrophobic molecules at the entrance of the active site pocket. The phosphonate inhibitor does not extend out to the protein surface and may therefore be insufficient for such a stabilization. The structures from four crystal forms of CALB that we have now solved indicate that the enzyme lacks a lid. This has prompted us to investigate the interfacial activation in CALB by biochemical means, and none could be detected (Martinelle *et al.*, 1995).

*Substrate Specificity and Stereoselectivity.* Although the overall structure and serine triad conformation are similar in all lipases, their substrate specificities and degrees of stereoselectivity differ widely. Substrate mapping of lipases has been carried out for secondary alcohols (Kazlauskas *et al.*, 1991; Santaniello *et al.*, 1992), and the general finding is that the stereoselectivity is higher if there is one small and one large substituent on the chiral carbon, rather than two of approximately equal size. Furthermore, all lipases and esterases display the same preference for a given enantiomer of secondary alcohols, and a general rule for predicting which enantiomer reacts faster that is valid for most substrates and lipases has been proposed (Kazlauskas *et al.*, 1991).

A structural explanation for the stereoselectivity of lipases towards secondary alcohols has been described in a study on *C. rugosa* lipase, based upon the structures of two enzyme complexes with chiral menthyl ester analogues (Cygler *et al.*, 1994). In the crystal structure of the enzyme complex with the analogue to the fast reacting (*R*)-menthyl ester, the catalytic histidine residue forms a hydrogen bond to the oxygen atom of the menthyl group. This hydrogen bond is lacking in the complex with the analogue to the slow-reacting (*S*)-menthyl ester. This missing hydrogen bond is taken to account for the slower reactivity of the (*S*)-menthyl esters. The present study is in agreement with these results and extends our understanding of the unusually high stereose-

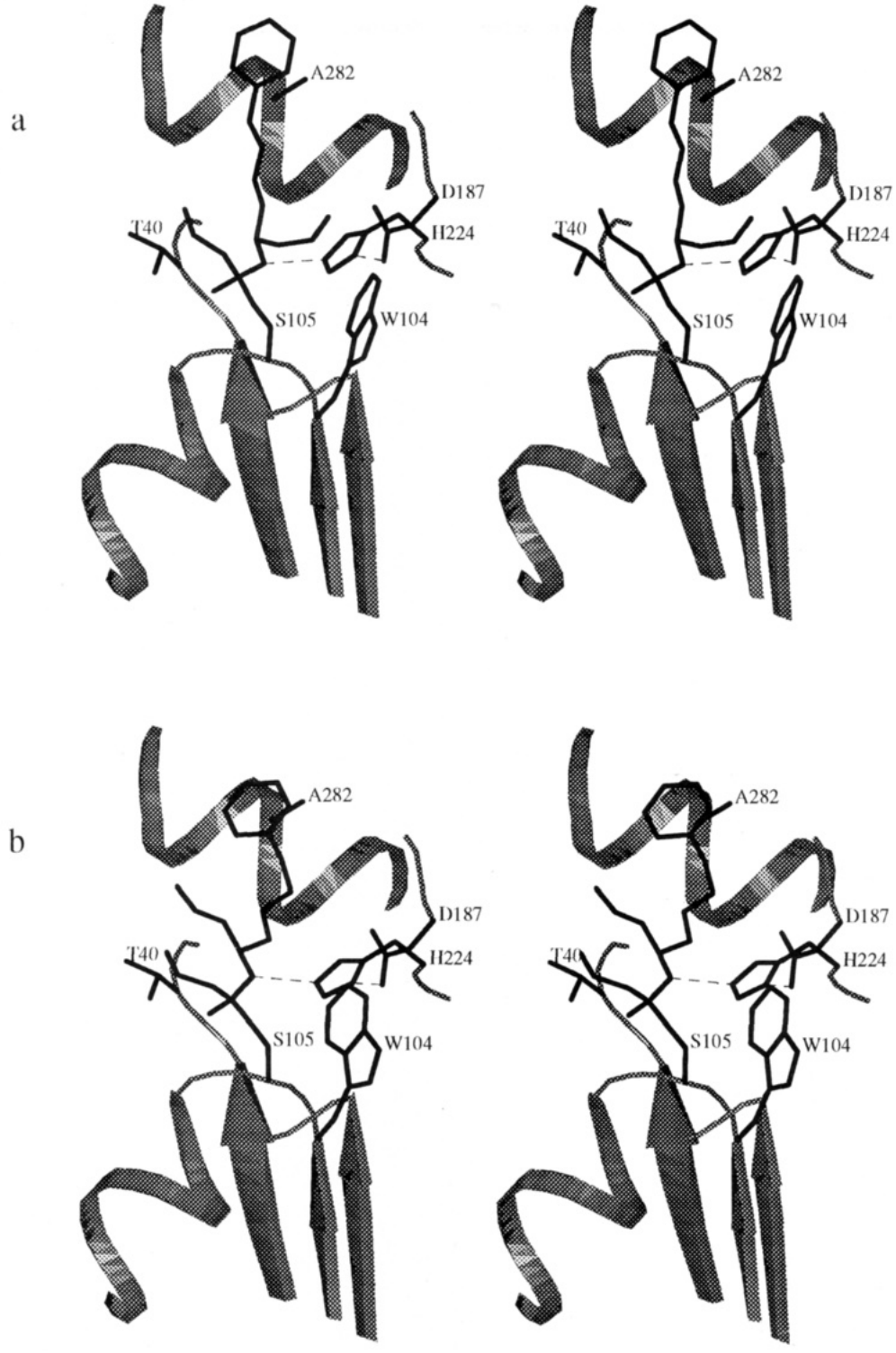


FIGURE 15: Substrate 2. The modeled structure of the butanoic ester intermediate after minimization of the structure with the lowest energy from the molecular dynamics simulation. (a) The *R* enantiomer of this substrate fits well into the active site pocket after a small movement of the side chain of Trp104. The long side chain of the alcohol is in a relaxed extended conformation. (b) The *S* enantiomer keeps the hydrogen bond to the histidine, but the large group extending from the chiral carbon of the alcohol has to make a curve in the active site pocket, forcing it into a strained conformation.

lectivity toward some secondary alcohols that has been demonstrated for CALB. Although the preference toward one of the enantiomers of secondary alcohols is similar for most lipases, the space available for the two substituents of the alcohol differs between enzyme species. We have investigated the alcohol side of the active site pocket with the enantiomers of two secondary alcohols. This has revealed a small and well-defined pocket suitable for accomodation of the small substituent of the fast-reacting enantiomer. This pocket is buried under a surface helix and delimited by the side chain of Trp104. The restricted volume of this pocket allows us to suggest which groups are likely to fit there. In the first substrate modeled, the phenylethyl octanoate complex, a methyl group fits easily into this pocket. The methoxymethyl group of the second substrate to be modeled is more troublesome and causes some close contacts with the protein. However, experimentally, it is still efficiently hydrolyzed with high stereoselectivity, and we,

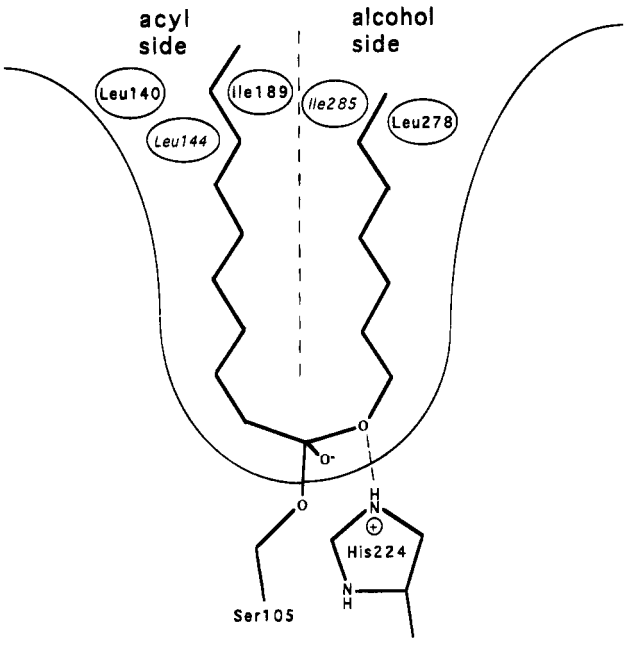


FIGURE 16: Active site pocket can be partitioned into two sides, an acyl side and an alcohol side, where the corresponding parts of the substrate will be located during catalysis. This conformational restriction is imposed on the substrate by the necessary transfer of a proton between the alcohol oxygen and the Nϵ of the active site histidine during catalysis.

therefore, assume that there is some flexibility of the protein in this region. The side chain of Trp104 is of great interest since it makes up the bottom of the stereospecificity pocket. This residue precedes the active site serine, and we believe it is structurally important since it forms a hydrogen bond from the nitrogen atom of its indole ring to the backbone oxygen of the active site histidine. In most other lipases, however, this residue is a histidine with an imidazole nitrogen at a position equivalent to that of the indole nitrogen. We believe, therefore, that this residue would make an interesting target for site-directed mutagenesis in many lipases. A single mutation of this tryptophan to a histidine in our model of CALB creates a larger pocket for a substrate side chain to occupy. The molecular dynamics simulations suggest that the critical hydrogen bond between the alcohol oxygen of the substrate and the active site histidine is retained not only for the *R* enantiomers of both substrates but also for the *S* enantiomer of the second subsrate. The high enantioselectivity for the second substrate is therefore more difficult to explain than for the first substrate.

Secondary alcohols have been widely used in reactions with lipases that display less pronounced stereoselectivity than CALB. For *R. miehei* lipase, molecular dynamics studies have been carried out to explain its stereoselectivity on these substrates (Norin *et al.*, 1994). The active site of this enzyme is more open and allows more flexibility for substrates to adopt suitable conformations. In *C. rugosa* lipase, the binding site for the small substituent is more accessible to the surface than in CALB. It has also been reported that this enzyme does not follow the prediction rule of enantioselectivity for acyclic secondary alcohols (Kazlauskas *et al.*, 1991). This means that the large substituent for the slow-reacting enantiomer of some of these more flexible substrates can be accommodated in the binding site for the small substituent. For the cyclic substrates, the prediction rule works well, which is also exemplified by the crystal structures of the menthyl ester analogues (Cygler *et al.*, 1994).

Work to examine the specificity pocket of CALB by further variation of the size of the groups extending from the chiral carbon is now in progress. Trials to crystallize chiral inhibitors to gain more insight into the structural features that govern the stereoselectivity of CALB will also be undertaken.

Substrates with a chiral center on the acyl side have been studied less with CALB as a catalyst. The stereoselectivity with respect to this side of the substrate is much lower than for the alcohol side (Quirós *et al.*, 1993; Sinisterra *et al.*, 1994). The proposed acyl side of the active site pocket is more spacious than the alcohol side, and it might be able to accommodate both enantiomers of such chiral acyl groups.

## ACKNOWLEDGMENT

We thank Dr. Fredrik Björkling, Novo Nordisk A/S, for providing us with the phosphonate inhibitor.

## REFERENCES

Besler, B. H., Merz, K. M. J., & Kollman, P. A. (1990) *J. Comput. Chem. 11*, 431−439.

Björkling, F., Godtfredsen, S. E., & Kirk, O. (1991) *TIBTech. 9*, 360−363.

Björkling, F., Godtfredsen, S. E., Kirk, O., Patkar, S. A., & Andersen, O. (1992) *Microb. Reagents Org. Synth., 1992*, 249−260.

Blow, D. M., Birktoft, J. J., & Hartley, B. S. (1969) *Nature 221*, 337−340.

Brady, L., Brzozowski, A. M., Derewenda, Z. S., Dodson, E., Dodson, G., Tolley, S., Turkenburg, J. P., Christiansen, L., Huge-Jensen, B., Norskov, L., Thim, L., & Menge, U. (1990) *Nature 343*, 767−770.

Brünger, A. T. (1990) *Acta Crystallogr. A46*, 46−57.

Brünger, A. T. (1992a) *X-PLOR. Version 3.1. A system for X-ray crystallography and NMR*, Yale University Press, New Haven CT.

Brünger, A. T. (1992b) *Nature 355*, 472−475.

Brünger, A. T., Krukowski, A., & Erickson, J. (1990) *Acta Crystallogr. A46*, 585−593.

Brzozowski, A. M., Derewenda, U., Derewenda, Z. S., Dodson, G. G., Lawson, D. M., Turkenburg, J. P., Björkling, F., Huge-Jensen, B., Patkar, S. A., & Thim, L. (1991) *Nature 351*, 491−494.

Collaborative Computational Project Number 4. (1994) *Acta Crystallogr. D50*, 760−763.

Cygler, M., Grochulski, P., Kazlaukas, R. J., Schrag, J. D., Bouthillier, F. B., Rubin, B., Serreqi, A. N., & Gupta, A. K. (1994) *J. Am. Chem. Soc. 116*, 3180−3186.

Derewenda, U., Swenson, L., Green, R., Wei, Y., Dodson, G. G., Yamaguchi, S., Haas, M. J., & Derewenda, Z. S. (1994a) *Nat. Struct. Biol. 1*, 36−47.

Derewenda, U., Swenson, L., Wei, Y., Green, R., Kobos, P. M., Joerger, R., Haas, M. J., & Derewenda, Z. S. (1994b) *J. Lipid Res. 35*, 524−534.

Desnuelle, P. (1972) *The Enzymes 7*, 575−616.

Engh, R. A., & Huber, R. (1991) *Acta Crystallogr. A47*, 392−400.

Fisher, R. G., & Sweet, R. M. (1980) *Acta Crystallogr. A36*, 755−760.

Franken, S. M., Rozeboom, H. J., Kalk, K. H., & Dijkstra, B. (1991) *EMBO J. 10*, 1297−1302.

Frykman, H., Öhrner, N., Norin, T., & Hult, K. (1993) *Tetrahedron Lett. 34*, 1367−1370.

Gillis, A. (1988) *J. Am. Oil Chem. Soc. 65*, 846−850.

Goodford, P. J. (1985) *J. Med. Chem. 28*, 849−857.

Grochulski, P., Li, Y., Schrag, J. D., Bouthillier, F., Smith, P., Harrison, D., Rubin, B., & Cygler, M. (1993) *J. Biol. Chem. 268*, 12843−12847.
Grochulski, P., Li, Y., Schrag, J. D., & Cygler, M. (1994) *Protein Sci. 3*, 82−91.
Hamlin, R. (1985) *Methods Enzym. 114*, 416−452.
Hjorth, A., Carriéré, F., Cudrey, C., Wöldike, H., Boel, E., Lawson, D. M., Ferrato, F., Cambillau, C., Dodson, G. G., Thim, L., & Verger, R. (1993) *Biochemistry 32*, 4702−4707.
IUBMB (1992) *Enzyme nomenclature*, Academic Press, London.
Jones, T. A., Zou, J.-Y., Cowan, S. W., & Kjeldgaard, M. (1991) *Acta Crystallogr. A47*, 110−119.
Kabsch, W. (1988) *J. Appl. Crystallogr. 21*, 916−924.
Kazlauskas, R. J., Weissfloch, A. N. E., Rappaport, A. T., & Cuccia, L. A. (1991) *J. Org. Chem. 56*, 2656−2665.
Kleywegt, G. J., & Jones, T. A. (1994a) *Acta Crystallogr. D50*, 178−185.
Kleywegt, G. J., & Jones, T. A. (1994b) in *From first map to final model* (Bailey, S., Hubbard, R., & Waller, D. A., Eds.) pp 59−66, SERC Daresbury Laboratory, Daresbury, U.K.
Lawson, D. M., Derewenda, U., Serre, L., Ferri, S., Szittner, R., Wei, Y., Meighen, E. A., & Derewenda, Z. S. (1994) *Biochemistry 33*, 9382−9388.
Martinelle, M., & Hult, K. (1995) *Biochim. Biophys. Acta 1251*, 191−197.
Martinelle, M., Holmquist, M., & Hult, K. (1995) *Biochim. Biophys. Acta 1258*, 272−276.
Martinez, C., DeGeus, P., Lauwereys, M., Matthyssens, G., & Cambillau, C. (1992) *Nature 356*, 615−618.
Matthews, B. W. (1968) *J. Mol. Biol. 33*, 491−497.
McPherson, A. (1982) in *Preparation and analysis of protein crystals*, pp 96−97, J. Wiley & Sons, Inc., New York.
Messerschmidt, A., & Pflugrath, J. W. (1987) *J. Appl. Crystallogr. 30*, 306−315.
Noble, M. E. M., Cleasby, A., Johnson, L. N., Egmond, M. R., & Frenken, L. G. J. (1993) *FEBS Lett. 331*, 123−128.
Norin, M., Hult, K., Mattson, A., & Norin, T. (1993) *Biocatalysis 7*, 131−147.
Norin, M., Haeffner, F., Achour, A., Norin, T., & Hult, K. (1994a) *Protein Sci. 3*, 1493−1503.
Norin, M., Haeffner, F., Hult, K., & Edholm, O. (1994b) *Biophys. J. 67*, 548−559.
Ollis, D. L., Cheah, E., Cygler, M., Dijkstra, B., Frolow, F., Franken, S. M., Harel, M., Remington, S. J., Silman, I., Schrag, J. D., Sussman, J. L., Verschueren, K. H. G., & Goldman, A. (1992) *Protein Eng. 5*, 197−211.
Patkar, S. A., Björkling, F., Zundel, M., Schülein, M., Svendsen, A., Heldt-Hansen, H. P., & Gormsen, E. (1993) *Ind. J. Chem. 32B*, 76−80.
Quirós, M., Sánchez, V. M., Brieva, R., Rebolledo, F., & Gotor, V. (1993) *Tetrahedron: Asymmetry 4*, 1105−1112.
Ryckaert, J.-P., Ciccotti, G., & Berendsen, H. J. C. (1977) *J. Comput. Phys. 23*, 327−341.
Santaniello, E., Ferraboschi, P., Grisenti, P., & Manzocchi, A. (1992) *Chem. Rev. 92*, 1071−1132.
Schrag, J. D., Li, Y., Wu, S., & Cygler, M. (1991) *Nature 351*, 761−764.
Sinisterra, J. V., Llama, E. F., del Campo, C., Cabezas, M. J., Moreno, J. M., & Arroyo, M. (1994) *J. Chem. Soc., Perkin Trans. 2*, 1333−1336.
Sussman, J. L., Harel, M., Frolow, F., Oefner, C., Goldman, A., Toker, L., & Silman, I. (1991) *Science 253*, 872−879.
Uppenberg, J., Patkar, S. A., Bergfors, T., & Jones, T. A. (1994a) *J. Mol. Biol. 235*, 790−792.
Uppenberg, J., Hansen, M. T., Patkar, S., & Jones, T. A. (1994b) *Structure 2*, 293−308.
van Tilbeurgh, H., Egloff, M.-P., Martinez, C., Rugani, N., Verger, R., & Cambillau, C. (1993) *Nature 362*, 814−820.
Waagen, V., Hollingsæter, I., Partali, V., Thorstad, O., & Anthonsen, T. (1993) *Tetrahedron: Asymmetry 4*, 2265−2274.
Wei, Y., Schottel, J. L., Derewenda, U., Swenson, L., Patkar, S., & Derewenda, Z. S. (1995) *Nat. Struct. Biol. 2*, 218−223.
Weiner, S. J., Kollman, P. A., Case, D. A., Singh, U. C., Ghio, C., Alagona, G., Profeta, S. J., & Weiner, P. A. (1984) *J. Am. Chem. Soc. 106*, 765−784.
Weiner, S. J., Kollman, P. A., Nguyen, D. T., & Case, D. A. (1986) *J. Comput. Chem. 7*, 230−252.
Winkler, F. K., D'Arcy, A., & Hunziker, W. (1990) *Nature 343*, 771−774.
Wright, C. S., Alden, R. A., & Kraut, J. (1969) *Nature 221*, 235−242.

BI951640V